Journal of Experimental and Theoretical Physics, Vol. 101, No. 3, 2005, pp. 401–409.
Translated from Zhurnal Éksperimental'noĭ i Teoreticheskoĭ Fiziki, Vol. 128, No. 3, 2005, pp. 464–475.

ATOMS, MOLECULES, OPTICS

Modified Phase Matching Conditions for Second Harmonic Generation in a Finite One-Dimensional Photonic Crystal near the Bragg Condition: Weak and Strong Diffraction

E. V. Petrov and B. I. Mantsyzov
Moscow State University, Moscow, 119992 Russia
e-mail: epetrov@genphys.phys.msu.ru; mants@genphys.phys.msu.ru
Received December 20, 2004

Abstract—Enhanced noncollinear second harmonic generation in a finite one-dimensional photonic crystal is analyzed theoretically under conditions of pump field localization near the Bragg reflection. It is shown numerically that phase-matched second-harmonic generation can be implemented in a finite one-dimensional photonic crystal that does not satisfy the conventional phase-matching conditions calculated for effective Bloch modes with narrow spectral lines. The intensity of the generated second-harmonic signal exceeds the second-harmonic intensity attained under the conventional phase-matching conditions by more than an order of magnitude. This phenomenon is explained by interference between Bloch modes having similar amplitudes, wavenumbers, and spectral widths. Since the spatial spectra of waves propagating in a bounded medium have finite widths, the broadened spectral lines of proximate effective Bloch modes resulting from Bragg diffraction of waves tuned to the first transmission resonances near the photonic band-gap edge overlap, merging into a spectral profile with center shifted relative to the original effective Bloch wavevectors. This effect leads to modified phase matching conditions for second harmonic generation in a finite photonic crystal, which are written for the centers of the spectral profiles resulting from modal overlap, rather than for individual effective wavevectors. Substantially different phase matching conditions are obtained for weakly and strongly diffracted beams, whereas conventional phase matching conditions hold only for transmitted signals in the case of weak diffraction. © *2005 Pleiades Publishing, Inc.*

1. INTRODUCTION

Recent development of new nonlinear optical materials, photonic crystals [1, 2], has motivated extensive studies of parametric conversion in periodic nonlinear structures [3]. Photonic crystal is an artificial structure with periodically modulated dielectric constant (in the general case, in three dimensions). When the modulation period is comparable to an optical wavelength, a light wave cannot propagate into the structure if its frequency or angle of incidence lies within a certain range called photonic band gap (PBG) [4]. Photonic crystals are characterized by strong localization of the energy of a pump (fundamental) beam whose frequency or angle of incidence corresponds to a PBG edge. The increase in pump energy density leads to higher amplitudes of polarization waves and, as a consequence, to higher intensities of Raman sidebands generated in parametric conversion processes. For one-dimensional photonic crystals, this effect was investigated in [5, 6]. We call it non-phase-matching enhancement. In [7], it was shown analytically that the energy of a localized pump wave can be proportional to the number of photonic-crystal periods cubed. Therefore, non-phase-matching enhancement provides a very efficient method for enhancing nonlinear wave interaction in periodically structured materials, whereas the intensities of signals generated in homogeneous media cannot increase faster than the sample length squared. It is well known that conversion of pump energy into Raman sidebands is efficient only when phase or group-velocity matching conditions are satisfied, as in birefringent crystals [8], artificial crystals with regular domain structure [9–11], or optical waveguides [12–14]. Since phase matching and non-phase-matching enhancement conditions are combined in photonic crystals [15–17], conversion efficiency can be additionally enhanced in photonic crystals as compared to homogeneous materials. For a photonic crystal about ten micrometers thick, the efficiency of energy conversion from fundamental into second-harmonic field can exceed 10% [18, 19], which is higher than the efficiency of nonlinear optical conversion in a homogeneous nondispersive medium of similar thickness. Strong spatial dispersion near the PBG edge [4] can compensate for the material dispersion in a photonic crystal, ensuring phase-matched interaction between fundamental and generated waves in nonlinear processes. We call this effect dispersion phase matching (DPM). Simultaneous fulfillment of the DPM and non-phase-matching enhancement conditions was predicted theoretically in [15] and demonstrated experimentally in [16] for second harmonic generation. Another mechanism of compensation of phase mismatch between interacting waves in photonic crystals

1063-7761/05/10103-0401$26.00

involves the reciprocal lattice vector and is known as quasi-phase-matching (QPM) [10]. QPM conditions are generally fulfilled for counterpropagating pump and signal waves, whereas DPM is characteristic of copropagating waves. Sum-frequency generation under QPM conditions combined with non-phase-matching enhancement conditions was demonstrated in [17]. Material dispersion can also be compensated for signals generated in nonlinear liquid crystals of certain types [20–22], which can essentially be treated as natural photonic crystals. However, the refractive-index modulation amplitude in these crystals is not sufficient for achieving significant non-phase-matching enhancement.

According to [15], second harmonic generation can be implemented in a photonic crystal under phase matching conditions for effective wavevectors [23] if the fundamental and second-harmonic frequencies are tuned, respectively, to the first and second transmission resonances relative to the corresponding PBG center frequencies. Experimental evidence of the corresponding second-harmonic intensity peak was obtained in [16, 24] for structures specially designed to meet these conditions. However, the efficiency of second harmonic generation under non-phase-matching enhancement conditions has never been analyzed for fundamental wave and second harmonic tuned to other transmission resonances. The parameters of periodic structures and pump beams corresponding to optimal efficiency of Raman sideband generation are generally calculated by using effective wavevectors [4, 23] in conventional phase matching conditions similar to those for waves propagating in infinite homogeneous media. In this method, the field propagating in a layered structure is represented as a superposition of Bloch modes characterized by effective wavevectors instead of Bloch vectors. However, a real photonic crystal cannot be treated as a homogeneous medium even approximately. The field inside a bounded crystal has a very complex structure consisting of Bloch modes with spectral widths $\Delta k \sim 2\pi/L$, where L is the sample length. Therefore, if the shift between two proximate Bloch modes with comparable amplitudes is approximately equal to Δk (when the pump is tuned near the PGB edge), then the corresponding spectral lines merge, and the resulting profile has a peak shifted relative to the effective wavevector. Accordingly, the phase matching conditions calculated for modes with finite spectral widths may be shifted relative to the phase matching conditions calculated by using effective wavevectors (corresponding to Bloch modes with narrow spectral lines), and the maximum shift is π/L. For example, the peak intensities and frequencies of the second-harmonic and sum-frequency signals measured in [17] were shifted relative to those corresponding to the exact phase conditions calculated for effective wavevectors.

In this study, we use a special noncollinear geometry to ensure non-phase-matching enhancement in a wide frequency range and apply the transfer matrix formalism [25] to demonstrate the possibility of efficient second harmonic generation in a thin one-dimensional photonic crystal when the fundamental-wave and second-harmonic first transmission resonances coincide. In this case, even though the conventional phase matching conditions calculated for effective wavevectors corresponding to Bloch modes with narrow spectral lines are not satisfied, the signal intensity exceeds that of the second harmonic satisfying the conventional phase matching conditions [15, 16]. This effect is explained by analyzing dynamics of coupled modes and taking into account the overlapping in both pump and signal spectra. We propose modified phase matching conditions written for the centers of profiles resulting from modal overlap in the spatial spectra of coupled waves. We show that optimal conditions for efficient coupling between the pump and signal waves are substantially different in the cases of strong and weak Bragg diffraction in a photonic crystal.

The paper is organized as follows. In Section 2, we formulate the problem, outline the method of solution, and describe the periodic structure to be examined. In Section 3, we analyze the spatial spectra of waves propagating through periodic structures. The results of Section 3 are used in Section 4 to explain the behavior of the frequency profiles of second-harmonic intensity obtained in the cases of weak and strong diffraction.

2. SECOND HARMONIC GENERATION NEAR THE EDGE OF THE PHOTONIC BAND GAP IN A BOUNDED PHOTONIC CRYSTAL

We consider second harmonic generation in a stack of N bilayers characterized by quadratic nonlinearity, with thicknesses d_1 and d_2 and complex frequency-dependent refractive indices $n_1(\omega)$ and $n_2(\omega)$, on an infinite substrate with complex refractive index n_{subs}. Their second-order susceptibilities $\chi_1^{(1)}$ and $\chi_2^{(2)}$ are assumed to be constant for simplicity (subscripts 1 and 2 refer to odd and even layers, respectively). Pump beams with frequencies ω_1 and ω_2 are incident from vacuum onto the crystal surface at arbitrary angles θ_1 and θ_2, respectively, to the normal vector. The z axis is aligned with the normal vector and directed into the crystal, the x axis is parallel to its surface, and the xz plane is the plane of incidence of the fundamental waves.

Owing to quadratic nonlinearity, a polarization wave with frequency $\omega_1 + \omega_2$ is created in the photonic crystal, which gives rise to a sum-frequency signal at $\omega_3 = \omega_1 + \omega_2$. The pump and sum-frequency fields inside the crystal, $\mathbf{E}_{1,2}(\mathbf{r}, t)$ and $\mathbf{E}_3(\mathbf{r}, t)$, and the input and output fields (in vacuum and substrate, respectively) are found by solving the nonlinear wave equation

$$\mathrm{rotrot}\mathbf{E} + \frac{1}{c^2}\frac{\partial^2 \mathbf{D}}{\partial t^2} = \frac{4\pi}{c^2}\frac{\partial^2 \mathbf{P}_{NL}}{\partial t^2}. \quad (1)$$

Here, $\mathbf{D}(\mathbf{r}, t) = n^2(\mathbf{r})\mathbf{E}(\mathbf{r}, t)$ is electric induction,

$$\mathbf{P}_{\mathrm{NL}}(\mathbf{r}, t) = \chi^{(2)} : \mathbf{E}(\mathbf{r}, t)\mathbf{E}(\mathbf{r}, t)$$

is the nonlinear polarization vector, and c is the speed of light in free space. In this study, the transfer matrix formalism [17, 25] is applied to solve Eq. (1) in the monochromatic plane-wave approximation for a prescribed pump field. This model is valid for pulses of duration up to 200–300 fs [6, 17] and weak nonlinearity. Under these assumptions, the transfer matrix formalism can be used to obtain an exact solution to Eq. (1) (with second spatial derivatives) describing the complex multiple-mode structure of localized fields in a thin photonic crystal.

Hereinafter, we consider the degenerate case of sum-frequency signal with $\omega_1 = \omega_2 = \omega$ and $\omega_3 = 2\omega$. To optimize the fundamental-wave parameters with respect to maximum generated signal intensity, we use the noncollinear beam geometry illustrated by Fig. 1a, which ensures fulfillment of the non-phase-matching enhancement condition in a wide frequency range. We vary ω and angle of incidence θ simultaneously to satisfy the non-phase-matching enhancement condition, i.e., to maximize the energy W of the field localized in the structure (Fig. 1b),

$$W = \int_0^t n^2(z)|E(z)|^2 dz,$$

where $z = 0$ and $z = L = N(d_1 + d_2)$ are the input and output surfaces of the photonic crystal. The mismatch parameters Δ_{DPM} and Δ_{QPM} corresponding, respectively, to dispersion phase matching and quasi-phase matching conditions are expressed in terms of effective wavevectors as

$$\Delta_{\mathrm{DPM}} = (k_{1z}^{\mathrm{eff}} + k_{2z}^{\mathrm{eff}} - k_{3z}^{\mathrm{eff}})L, \quad (2)$$

$$\Delta_{\mathrm{QPM}} = (k_{1z}^{\mathrm{eff}} + k_{2z}^{\mathrm{eff}} + k_{3z}^{\mathrm{eff}} - Hl)L, \quad (3)$$

where k_{zt}^{eff} denotes the z components of the pump (i = 1, 2) and signal (i = 3) waves, $H = 2\pi/(d_1 + d_2)$ is the magnitude of the reciprocal lattice vector, and l is an integer called quasi-phase-matching order. Expression (2) is analogous to the phase mismatch for a homogeneous medium, while the term proportional to Hl in (3) takes into account the contribution of Bloch modes due to Bragg diffraction in a periodic structure. The parameters in (2) and (3) vary with ω and θ. Phase matching corresponds to

$$\Delta_{\mathrm{DPM}}, \Delta_{\mathrm{QPM}} \le \pi/2. \quad (4)$$

Since the fundamental waves have equal frequencies, the corresponding wavevectors are symmetric relative to the normal: $\theta_1 = +\theta_0$ and $\theta_2 = -\theta_0$, where the angle of incidence θ_0 ensures non-phase-matching enhancement for a particular ω. Since the tangential components of the electric field vectors are continuous across layer boundaries [23], the "angle of incidence" θ_3 for the second harmonic is zero for any ω.

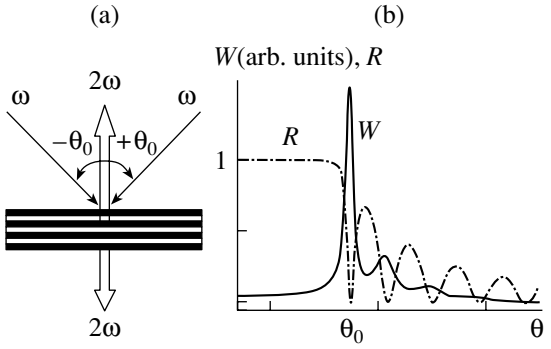

Fig. 1. Second harmonic generation: (a) noncollinear geometry; (b) reflectivity R (dash-dot curve) and energy W of localized electric field (solid curve) of the pump beam vs. angle of incidence θ (θ_0 corresponds to non-phase-matching enhancement).

Figure 2a shows the intensities $I^{(+)}$ and $I^{(\angle)}$ of the transmitted and reflected second-harmonic signals in the geometry considered here versus normalized frequency for the stack of 15 bilayers with $n_1(\omega)$ and $n_2(\omega)$ corresponding to AlO_x and AlGaAs (nonlinear optical material), respectively [16]. Here, $d_1 = \lambda_0/3n_1(\omega_0)$ and $d_2 = 3\lambda_0/4n_2(\omega_0)$, where $\lambda_0 = 2\pi c/\omega_0$ and ω_0 is a reference frequency; the substrate is vacuum. The intensity $I^{(\pm)}$ is normalized to that of the second-harmonic signal with frequency $2\omega_0$ generated in a homogeneous nondispersive medium of thickness $D = Nd_2$ with refractive index $n_2(\omega_0)$. Figures 2b and 2c show, respectively, the second-harmonic reflectivity and the phase mismatch parameters Δ_{DPM} and Δ_{QPM}, respectively. The phase matching order is l = 4, and all waves are s-polarized.

The second-harmonic intensity spectrum shown in Fig. 2a exhibits two peaks whose locations are indicated by vertical dash-dot lines A and B. The former corresponds to the zero of Δ_{DPM} associated with the second transmission resonance (relative to the second-harmonic PBG center frequency). The existence of this peak was demonstrated in [15, 16, 24]. The latter is associated with the first second-harmonic transmission resonance and is not related to any zero of Δ_{DPM} or Δ_{QPM}. This intensity peak is more than an order of magnitude higher than the former one; i.e., the corresponding phase matching conditions cannot be formulated in terms of effective wavevectors corresponding to Bloch modes with narrow spectral lines, as in (2) or (3). Its location should therefore be explained by analyzing a multiple-mode structure in order to find phase matching conditions different from (2)–(4).

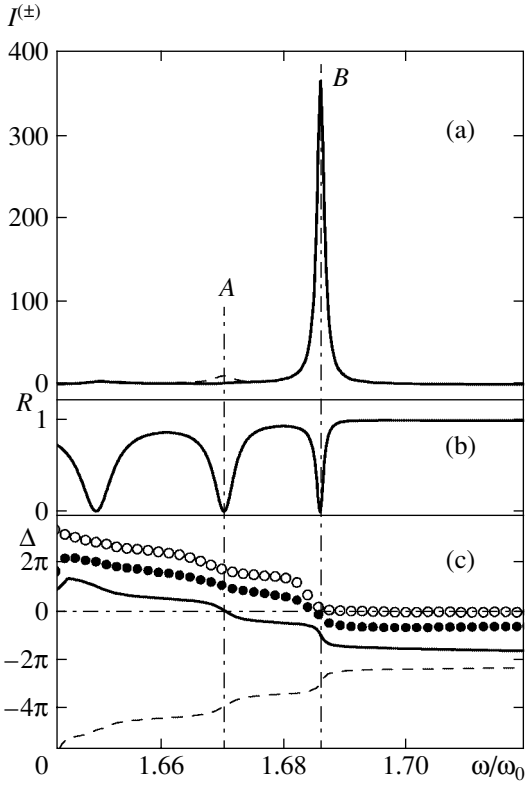

Fig. 2. Normalized frequency dependence: (a) normalized intensities $I^{(+)}$ and $I^{(-)}$ of the transmitted and reflected second-harmonic signals (solid and dashed curves, respectively); (b) second-harmonic reflectivity R; (c) phase mismatch parameters Δ_{DPM} (solid curve) and Δ_{QPM} (dashed curve); $\Delta^{(+)}$ (●) and $\Delta^{(-)}$ (○). Vertical dash-dot lines A and B indicate the peak second-harmonic intensities corresponding to the second and first transmission resonances, respectively.

3. SPATIAL SPECTRA OF WAVES DIFFRACTED NEAR THE PHOTONIC BAND-GAP EDGE

In the model presented above, an effective wavevector $k^{\text{eff}}(\omega)$ is calculated to characterize the propagation of a wave with frequency ω through a multilayered stack. The linear properties of a photonic crystal are characterized by a dispersion curve shown in Fig. 3 (right solid branch). Any layered structure generates a reflected (backward) wave. Since the magnitude of the corresponding wavevector is equal to that of the forward wave, the reflected-wave dispersion curve is symmetric to the forward-wave one relative to the ω axis (left solid branch in Fig. 3). However, Bragg diffraction in a periodic structure must give rise to a Bloch wave related to the incident wave by the Bragg condition $\mathbf{k}_2 = \mathbf{k} + m\mathbf{H}$, where m is the number of the PBG responsible for diffraction; i.e., in addition to waves with wavevectors k^{eff} and $-k^{\text{eff}}$, there must exist Bragg-diffracted waves with $k^{\text{eff}} - mH$ and $-k^{\text{eff}} + mH$ (see Fig. 3). Thus, we must consider four waves propagating in a photonic crystal if diffraction is to be taken into account: two forward and two backward ones.

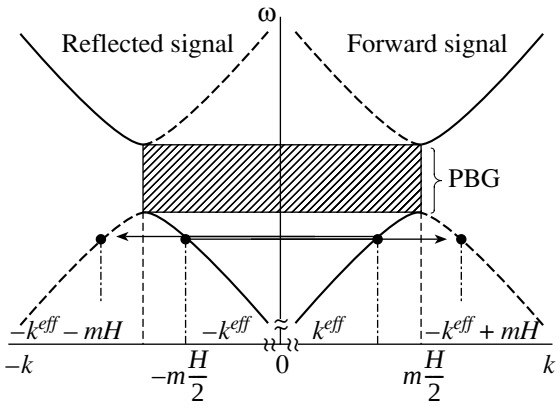

Fig. 3. Dispersion curves for forward (right) and reflected (left) signals in single-mode approximation (solid curves) and for diffracted signals. The hatched region corresponds to PBG. Dots on dispersion curves correspond to the wavenumbers of the forward (k^{eff}], backward ($-k^{\text{eff}}$), and Bragg-diffracted ($k^{\text{eff}} - mH$, $-k^{\text{eff}} + mH$) waves.

The existence of waves with wavenumbers $k^{\text{eff}} - mH$ and $-k^{\text{eff}} + mH$ is easy to demonstrate for a structure with continuous dielectric constant $\varepsilon(z)$, because neither Fourier series expansion of solutions nor their matching at the points of discontinuity is required in this case. Since wave propagation in periodic structures is governed by qualitatively similar relations, we can consider a crystal with harmonically modulated dielectric constant:

$$\varepsilon(z) = \begin{cases} \varepsilon_0, & z \notin [0, L], \\ \varepsilon_0[1 + \mu\cos(Hz)], & z \in [0, L], \end{cases}$$

where ε_0 is the background dielectric constant, μ is the modulation depth, $H = 2\pi/d$ is the reciprocal lattice vector, d is the modulation period, $L = \Lambda N$ is the crystal length, and $z = 0$ and $z = L$ are the input and output ends of the modulated crystal. The electric field distribution $E(z)$ in a linear medium is found by solving Eq. (1) with zero right-hand side [23].

Within the interval $[0, L]$, the electric field of a plane electromagnetic wave with frequency ω can be represented as

$$E(r, t) = E_0(z)\exp[i(\omega t - k_x x)]. \qquad (5)$$

where $k_x = k_0\sin\theta$ is the tangential component of the wavevector, $k_0 = \omega/c$ is the wavevector magnitude in free space, $k = k_0\sqrt{\varepsilon_0}$ is the wavevector magnitude in the medium, and θ is the angle between the wave propagation direction and the z axis. The complex amplitude $E_0(z)$ is expressed as

$$E_0(z) = E_+(z) + E_-(z) = A_+(z)\exp(ik_z z) + A_-(z)\exp(-ik_z z), \quad (6)$$

where $A_+(z)$ and $A_-(z)$ denote the amplitudes of the forward and backward waves, respectively, and

$$k_z = k_0\sqrt{\varepsilon_0 - \sin^2\theta}$$

is the z component of the pump wavevector. We assume that the dielectric-constant modulation depth is sufficiently small to satisfy the condition for slowly varying amplitudes,

$$\left|\frac{d^2A_\pm}{dz^2}\right| \ll \left|2k_z\frac{dA_\pm}{dz}\right|.$$

If the diffracted waves are tuned near the edge of the first PBG, then the parameter $\delta = k_z - H/2$ is a small quantity.

Substituting (5) and (6) into (1) (with $\mathbf{P}_{NL}$ set to zero), neglecting the fast-oscillating terms, and separating the terms containing $\exp(ik_z z)$ and $\exp(-ik_z z)$, we obtain the system of differential equations

$$\frac{d}{dz}A_+ = i\frac{\mu k^2}{4k_z}A_-\exp(-2i\delta z),$$
$$\frac{d}{dz}A_- = -i\frac{\mu k^2}{4k_z}A_+\exp(2i\delta z), \quad (7)$$

subject to the boundary conditions

$$A_+(z=0) = A_+^0, \quad A_-(z=L) = 0,$$

where A_+^0 is the incident intensity on the left-hand boundary between the homogeneous and modulated media, and the latter condition means that no beam is incident on the right-hand boundary.

Substituting the solution to (7) into (6), we obtain the following expressions for the forward and backward electric field amplitudes:

$$E_+(z) = \frac{\alpha\cos[\alpha(L-z)] - i\delta\sin[\alpha(L-z)]}{\alpha\cos(\alpha L) - i\delta\sin(\alpha L)} \times A_+^0\exp\left(i\frac{H}{2}z\right), \quad (8)$$

$$E_-(z) = i\frac{\mu k^2}{4k_z}\frac{\sin[\alpha(L-z)]}{\alpha\cos(\alpha L) - i\delta\sin(\alpha L)} \times A_+^0\exp\left(-i\frac{H}{2}z\right), \quad (9)$$

where

$$\alpha = \sqrt{\delta^2 - \left(\frac{\mu k^2}{4k_z}\right)^2}.$$

We rewrite the real values of the electric field strengths given by (8) and (9) as

$$\mathrm{Re}[E_+(z)] = \frac{1}{4\xi}\Big\{(\alpha+\delta)^2\cos(\beta_+ z) + (\alpha-\delta)^2\cos(\beta_- z) - \left(\frac{\mu k^2}{4k_z}\right)^2\cos(2\alpha L) \times [\cos(\beta_+ z) + \cos(\beta_- z)] - \left(\frac{\mu k^2}{4k_z}\right)^2\sin(2\alpha L)[\sin(\beta_+ z) - \sin(\beta_- z)]\Big\}A_+^0, \quad (10)$$

$$\mathrm{Re}[E_-(z)] = \frac{1}{4\xi}\frac{\mu k^2}{4k_z}\{(\alpha-\delta)\cos(-\beta_+ z) - (\alpha+\delta)\cos(-\beta_- z) + (\alpha+\delta)\cos(2\alpha L)\cos(-\beta_+ z) - (\alpha-\delta)\cos(-\beta_- z) - (\alpha+\delta)\sin(2\alpha L)\sin(-\beta_+ z) - (\alpha-\delta)\sin(2\alpha L)\sin(-\beta_- z)\}A_+^0. \quad (11)$$

where

$$\xi = \alpha^2\cos^2(\alpha L) + \delta^2\sin^2(\alpha L),$$
$$\beta_+ = \frac{H}{2} + \alpha, \quad \beta_- = \frac{H}{2} - \alpha.$$

Expressions (10) and (11) demonstrate that the field propagating in medium with modulated dielectric constant consists of four waves, with wavenumbers β_+, β_- and $-\beta_+$, $-\beta_-$ corresponding to forward and backward waves, respectively, i.e., to k^{eff}, $-k^{\mathrm{eff}} + mH$ and $-k^{\mathrm{eff}}$, $k^{\mathrm{eff}} - mH$ with $m = 1$. Since any wave propagating in a bounded photonic crystal has a finite spectral width estimated as $2\pi/L$, the modes with spectral lines separated by Δk overlap and the lines merge into a profile with center shifted relative to their respective centers if

$$\Delta k \le 2\pi/L. \quad (12)$$

Let us show that the spectral components of a signal tuned to the first transmission resonance (relative to the PBG center frequency) satisfy condition (12).

The reflectivity R for a periodic structure is expressed as

$$R = \left|\frac{E_-(z=0)}{E_+(z=0)}\right|^2 = \frac{\sin^2(\alpha L)}{\left(\frac{4\alpha k_z}{\mu k^2}\right)^2 + \sin^2(\alpha L)}.$$

Transmission resonances are defined by the condition $R = 0$, i.e.,

$$\alpha = \frac{\pi}{L}n, \quad n = 1, 2, 3, \ldots,$$

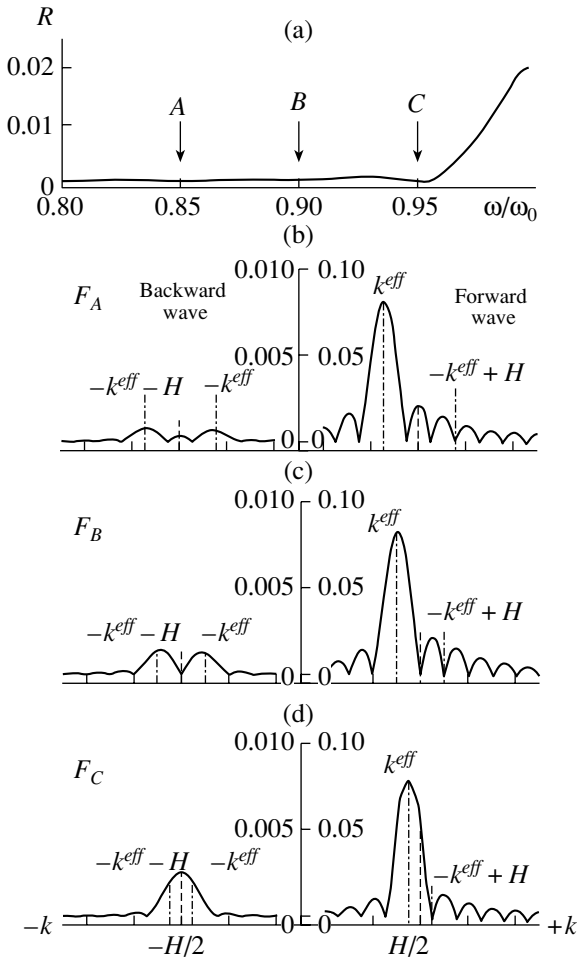

Fig. 4. Weak Bragg diffraction in a structure with cosinusoidally modulated dielectric constant: (a) reflectivity vs. normalized frequency. Spatial spectra of the forward and backward waves for pump beams tuned to (b) third, (c) second, and (d) first transmission resonances (*A*, *B*, and *C*, respectively). Vertical dashed and dash-dot lines indicate, respectively, *H*/2 components and the effective wavevectors of forward, backward, and diffracted waves calculated in the single-mode approximation.

where n is the number of a resonance, and the corresponding wavenumbers are

$$\beta_+ = \frac{H}{2} + \frac{\pi n}{L}, \quad \beta_- = \frac{H}{2} - \frac{\pi n}{L}.$$

Accordingly, $\Delta k = |\beta_+ - \beta_-| = 2\pi n/L$, which entails $\Delta k = 2\pi/L$ for the first transmission resonance, in agreement with condition (12). Thus, the modes centered at β_+ and β_- substantially overlap.

As an example, we consider second harmonic generation in the stack of 20 bilayers with $\Lambda/\lambda_0 = 0.25$, $\varepsilon_0 = 4$, and $\mu = 0.01$ (which corresponds to weak Bragg diffraction) in the case of normal beam incidence. Figure 4a shows the reflectivity plotted versus normalized wave frequency for this structure. The third, second, and first transmission resonances are indicated by *A*, *B*, and *C*, respectively. Figures 4b–4d show the spatial spectra

$$F(k) = \left| \frac{1}{2\pi L} \int_0^L \mathrm{Re}[E_\pm(z)] \exp(ikz) dz \right|,$$

plotted versus k normalized to $2\pi/L$ for waves tuned to the resonances *A*, *B*, and *C*, respectively. Here, the spectra of $E_-(z)$ and $E_+(z)$ correspond to $k < 0$ and $k > 0$, respectively; vertical dash-dot lines, to $k^{\mathrm{eff}} - mH$, $-k^{\mathrm{eff}}$, k^{eff}, and $-k^{\mathrm{eff}} + mH$ with $m = 1$. Figures 4b and 4c demonstrate that the reflected-wave spectrum contains two lines of equal intensity centered at $k^{\mathrm{eff}} - mH$ and $-k^{\mathrm{eff}}$, owing to diffraction of the incident wave. The spectrum of the forward wave contains only the component centered at k^{eff}, whereas the one centered at $-k^{\mathrm{eff}} + mH$ (due to reflected-wave diffraction) is absent in the case of weak diffraction, because $|E_-(z)| \sim \mu$.

A totally different reflected-wave spectrum is obtained for diffraction near the first transmission resonance *C* (Fig. 4d). As shown analytically above, the lines corresponding to $k^{\mathrm{eff}} - mH$ and $-k^{\mathrm{eff}}$ overlap and merge into a single line. Figure 4d demonstrates that the resulting reflected-wave line is centered at $mH/2$, whereas the spectrum of the forward wave is still centered at k^{eff}.

To analyze the case of strong diffraction, we find the spatial spectra of waves propagating in a medium with cosinusoidally modulated dielectric constant having 4
the parameters specified above, except for $\mu = 0.5$. The equations for slowly varying amplitudes are not applicable in this case, and the field distributions found numerically by using the transfer matrix formalism. Figure 5 shows the corresponding reflectivity and the spatial spectra of the backward and forward waves plotted in the same coordinates as those in Fig. 4.

Figure 5 demonstrates that the spectra of reflected waves are qualitatively similar in the cases of both weak and strong diffraction, differing only in amplitude, whereas the forward wave has a distinct component characterized by $-k^{\mathrm{eff}} + mH$ in the latter case. Its intensity is higher at the transmission resonance *B* (Fig. 5c) as compared to *A* (Fig. 5b), because Bragg reflection becomes stronger as the pump frequency is tuned closer to the PBG. Owing to the higher amplitude of the component with $-k^{\mathrm{eff}} + mH$, the center of the spectral profile resulting from modal overlap for a wave tuned to the first transmission resonance *C* is shifted from k^{eff} in the direction of $mH/2$.

The results of this section concerning wave-coupling efficiency in second harmonic generation can be summarized as follows. Due to the spectral shifts of the coupled waves involved in second harmonic generation near the corresponding PBG edge, phase matching conditions (2)–(4) do not hold for the reflected wave in the case of weak diffraction and for both reflected and forward waves in the case of strong diffraction. Thus, the

degree of spectral overlap of the coupled waves should be taken into account in determining optimal conditions for second harmonic generation. Since the highest efficiency of coupling between the fundamental waves and the second-harmonic signal is attained when the sum of the wavenumbers of the strongest fundamental-wave components (i.e., the wavenumber of the nonlinear polarization wave) corresponds to the center of the second-harmonic spectral profile, the modified mismatch parameters

$$\Delta^{(\pm)} = (\bar{k}_1^{(\pm)} + \bar{k}_2^{(\pm)} - \bar{k}_3^{(\pm)})L, \quad (13)$$

expressed in terms of the centers of broadened spectral profiles should be used instead of (2) and (3), and the modified phase matching conditions are written as

$$\Delta^{(\pm)} \le \pi/2 \quad (14)$$

where the superscripts (+) and (–) correspond to the forward and reflected pump ($i = 1, 2$) and signal ($i = 3$) waves.

In particular, the centers of the reflected-wave spectra in the case of strong diffraction of waves tuned near the first transmission resonance are given by the exact expression $\bar{k}_i^{(-)} = m_i H/2$, where m_i is the number of the corresponding PBG. Accordingly, the mismatch parameters defined by (13) can be written for both reflected and transmitted waves as follows:

$$\Delta^{(\pm)} = (m_1 + m_2 - m_3)\frac{HL}{2}.$$

Figure 2 illustrates strong diffraction near the PBGs with $m_{1,2} = 2$ and $m_3 = 4$, in which case we have $\Delta^{(\pm)} = (2 + 2 - 4)HL/2 = 0$; i.e., the phase matching conditions are satisfied exactly. This explains the existence of a second-harmonic intensity peak at the point *B* in Fig. 2a. Parameters (13) are shown as functions of frequency for the forward (closed circles) and reflected (open circles) waves in Fig. 2c, for which the centers of spectral profiles were determined directly from the computed spatial spectra. It is clear that phase matching conditions (14) for broadened spectral lines hold near the first transmission resonances.

4. SECOND HARMONIC GENERATION NEAR THE POINT OF FORBIDDEN BRAGG REFLECTION: WEAK AND STRONG DIFFRACTION

Let us demonstrate that modified phase matching conditions (13), (14) hold for second harmonic generation near the point of so-called forbidden Bragg reflection, which is observed when $2\mathbf{k} = m\mathbf{H}$ for a wave propagating through a multilayer stack, whereas each individual layer can transmit light without reflection. In this case, total transmission occurs instead of the total reflection dictated by the Bragg condition. In particular, forbidden Bragg reflection is observed when a beam is normally incident on a stack of alternating layers of two types whose optical thicknesses are multiples of the beam half-wavelength λ: $d_i = p\lambda/2n_i$, where *p* is an integer and n_i ($i = 1, 2$) are the refractive indices of the layers.

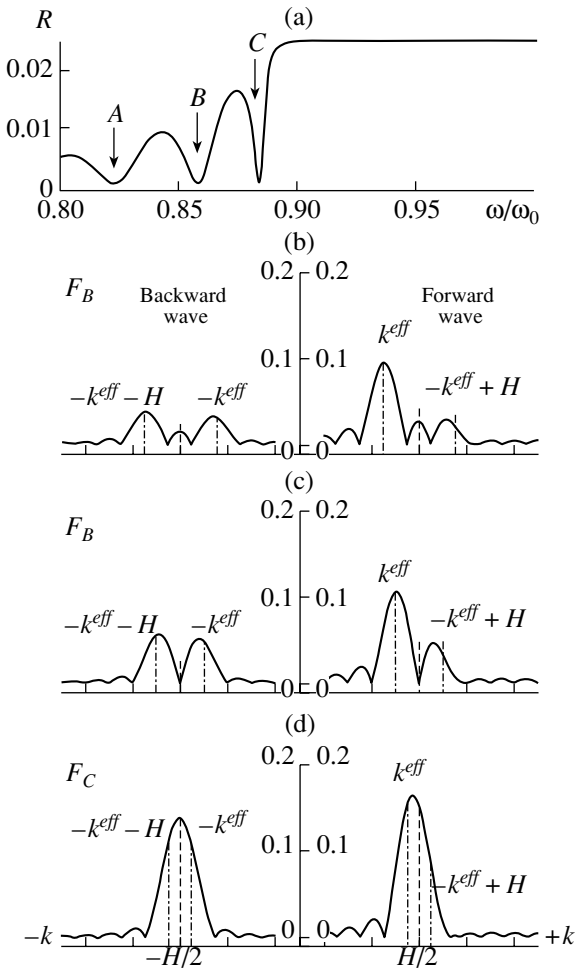

Fig. 5. Strong Bragg diffraction: (a) reflectivity vs. normalized frequency; (b)–(d) spatial spectra under the corresponding conditions specified in Fig. 4.

Let us examine the variation of the intensity $I^{(\pm)}$ with increasing refractive-index contrast $\Delta n = |n_1 - n_2|$ for the second harmonic generated near the point of forbidden Bragg reflection for waves with frequency 2ω when the incident wave is tuned near the PBG edge. As an example, we consider noncollinear second harmonic generation (see Fig. 1) in the stacks of 15 bilayers with $d_{1,2} = 3\lambda_0/4n_{1,2}$, $n_1 = n_{subs} = 1$, and different n_2 for the nonlinear even layers in the absence of material dispersion.

Figures 6a, 6b, and 6c show the intensities $I^{(+)}$ (left ordinate axes) and $I^{(-)}$ (right ordinate axes) of the forward and reflected second-harmonic signals, the second-harmonic reflectivity *R*, and the mismatch parameters Δ_{DPM} and $\Delta^{(+)}$ given by (2) and (13) for $n_2 = 1.1$

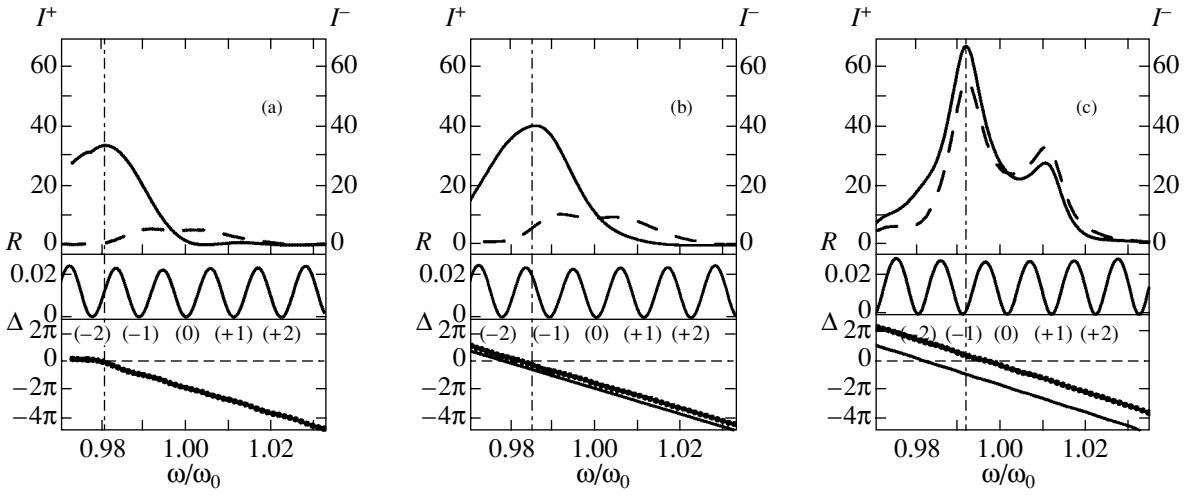

Fig. 6. Normalized intensities $I^{(+)}$ and $I^{(-)}$ of the transmitted and reflected second-harmonic signals (solid and dashed curves, respectively), second-harmonic reflectivity R, and phase mismatch parameters Δ_{DPM} (solid curves) and $\Delta^{(+)}$ (●) vs. normalized frequency for refractive-index contrast $\Delta n = 1.1$ (a), 1.3 (b) and 1.5 (c). Vertical dash-dot lines indicate peak intensities of transmitted second-harmonic signal.

(weak diffraction), 1.3 (intermediate case), and 1.5 (strong diffraction), respectively. The locations of peaks of $I^{(+)}(\omega)$ on the frequency axis are indicated by vertical dash-dot lines. The intensities are normalized as in Fig. 2. For the photonic crystal with the parameters specified above, forbidden Bragg reflection is observed if the second-harmonic frequency $2\omega_0$ corresponds to the central transmission resonance in the frequency dependence of R (denoted by (0) in Fig. 6). The first, second, etc. transmission resonances on its left and right (denoted by (–1), (–2), (+1), and (+2)) are analogous to those near the PBG in terms of both field distribution and spectral profiles.

In Fig. 6a, the point of maximum intensity of the forward second-harmonic signal coincides with the zeros of the mismatch parameters Δ_{DPM} and $\Delta^{(+)}$. By virtue of the beam geometry, the spatial spectra of both forward and backward waves are analogous to those in Fig. 4d. Accordingly, the spectrum of the forward wave is centered at $2k_{1z}^{\text{eff}}$, where k_{1z}^{eff} is the z component of the pump wavevector, and the curves of Δ_{DPM} and $\Delta^{(+)}$ coincide. The second-harmonic spectra at (±2) and (±1) are similar in form to those in Figs. 4c and 4d, respectively. Thus, modified phase matching conditions (14) hold for the forward signal near resonance (–2), where the strongest spectral components of the coupled waves overlap, and for the reflected signal near resonances (±1) and the point of forbidden Bragg reflection.

In the case of intermediate diffraction (see Fig. 6b), the reflected signal exhibits a qualitatively similar behavior, with a higher second-harmonic intensity due to stronger diffraction. The peak of the forward second-harmonic intensity is shifted to the right from the point where $\Delta_{DPM} = 0$, and the curves of $\Delta_{DPM}(\omega)$ and $\Delta^{(+)}(\omega)$ do not coincide. These changes are explained by appreciable contributions of the modes centered at $-k_z^{\text{eff}} + mH$ to the spectra of linear and nonlinear forward waves. The zero of $\Delta^{(+)}$ coincides with the point of maximum $I^{(+)}$.

In the case illustrated by Fig. 6c, the components centered at $-k_z^{\text{eff}} + mH$ strongly contribute to the spectra of the forward waves. The spectral profiles resulting from modal overlap at the fundamental-wave first transmission resonances are very similar in form to those shown in Fig. 5d, and their centers are located almost exactly at $mH/2$. Accordingly, the peak intensities of both forward and backward second-harmonic signals correspond to transmission resonances (±1).

5. CONCLUSIONS

Second harmonic generation is considered as an example to examine optimal conditions for nonlinear wave coupling in a finite one-dimensional photonic crystal in the cases of strong and weak Bragg diffraction. Special noncollinear beam geometry is used to meet the non-phase-matching enhancement conditions for the second-harmonic signal and determine the wave parameters corresponding to the most accurate simultaneous fulfillment of phase matching conditions. When the second harmonic is generated near the PBG or the point of forbidden Bragg reflection, the phase matching conditions for forward waves in the case of strong diffraction and for reflected waves in the cases of both strong and weak diffraction in a bounded medium differ from the corresponding conventional phase conditions. The modified phase matching conditions proposed here for a finite photonic crystal are written for the centers of

the spatial spectral profiles resulting from the overlap of broadened lines, rather than for the effective wavevectors of individual Bloch modes. These modified conditions are used to explain the enhanced phase-matched second-harmonic generation predicted in this study in the case when the fundamental-wave and second-harmonic first transmission resonances coincide. The results obtained here can also be used to analyze conditions for efficient conversion by different mechanisms (parametric amplification, Raman scattering, etc.) in finite photonic crystals.

ACKNOWLEDGMENTS

This work was supported by the Russian Foundation for Basic Research, project no. 04-02-16866.

REFERENCES

1. E. Yablonovitch, J. Mod. Opt. **41**, 173 (1994).
2. K. Sakoda, *Optical Properties of Photonic Crystals* (Springer, Berlin, 2001).
3. *Nonlinear Photonic Crystals*, Ed. by R. E. Slusher and B. J. Eggleton (Springer, Berlin, 2003).
4. A. Yariv and P. Yeh, J. Opt. Soc. Am. **67**, 438 (1977).
5. M. Scalora, M. J. Bloemer, A. S. Manka, *et al.*, Phys. Rev. A **56**, 3166 (1997).
6. A. V. Balakin, D. Bushe, V. A. Bushuev, *et al.*, Pis'ma Zh. Éksp. Teor. Fiz. **70**, 718 (1999) [JETP Lett. **70**, 725 (1999)].
7. E. V. Petrov, V. A. Bushuev, and B. I. Mantsyzov, Izv. Ross. Akad. Nauk, Ser. Fiz. **66**, 1787 (2002).
8. J. A. Giordmaine, Phys. Rev. Lett. **8**, 19 (1962).
9. J. A. Armstrong, N. Bloembergen, J. Ducuing, and P. S. Pershan, Phys. Rev. **127**, 1918 (1962).
10. M. M. Fejer, G. A. Magel, D. H. Jundt, and R. L. Byer, IEEE J. Quantum Electron. **28**, 2631 (1992).
11. A. S. Chirkin, V. V. Volkov, G. D. Laptev, and E. Yu. Morozov, Kvantovaya Élektron. (Moscow) **30**, 847 (2000).
12. Y. Fujii, B. S. Kawasaki, K. O. Hill, and D. C. Johnson, Opt. Lett. **5**, 48 (1980).
13. Y. Ohmori and Y. Sasaki, Appl. Phys. Lett. **39**, 466 (1981).
14. G. Agrawal, *Nonlinear Fiber Optics* (Academic, New York, 1995; Mir, Moscow, 1996).
15. M. Centini, C. Sibilia, M. Scalora, *et al.*, Phys. Rev. E **60**, 4891 (1999).
16. Y. Dumeige, I. Sagnes, P. Monnier, *et al.*, J. Opt. Soc. Am. B **19**, 2094 (2002).
17. A. V. Balakin, V. A Bushuev, B. I. Mantsyzov, *et al.*, Phys. Rev. E **63**, 046 609 (2001).
18. G. D'Aguanno, M. Centini, M. Scalora, *et al.*, Phys. Rev. E **64**, 016 609 (2001).
19. B. I. Mantsyzov, E. V. Petrov, E. B. Tereshin, and V. A. Trofimov, Izv. Ross. Akad. Nauk, Ser. Fiz. **68**, 1710 (2004).
20. I. D. Olenik and M. Copic, Phys. Rev. E **56**, 581 (1997).
21. V. A. Belyakov, Pis'ma Zh. Éksp. Teor. Fiz. **70**, 793 (1999) [JETP **70**, 811 (1999)].
22. J.-G. Yoo, S.-W. Choi, H. Hoshi, *et al.*, Jpn. J. Appl. Phys. Lett. **36**, L1168 (1997).
23. M. B. Vinogradova, O. V. Rudenko, and A. P. Sukhorukov, *The Theory of Waves* (Nauka, Moscow, 1979) [in Russian].
24. Y. Dumeige, P. Vidakovic, S. Sauvage, *et al.*, Appl. Phys. Lett. **78**, 3021 (2001).
25. D. S. Bethune, J. Opt. Soc. Am. B **6**, 910 (1989).

Translated by A. Betev

SPELL: 1. counterpropagating, 2. copropagating, 3. sideband, 4. cosinusoidally